J Therm Anal Calorim (2017) 129:895–903
DOI 10.1007/s10973-017-6204-9

# Thermo-derivative analysis of Al–Si–Cu alloy used for surface treatment

**Krzysztof Labisz[1] · Jarosław Konieczny[1] · Sebastian Jurczyk[3] · Tomasz Tański[2] · Mariusz Krupiński[2]**

Received: 19 June 2016 / Accepted: 15 February 2017 / Published online: 1 March 2017


**Abstract** The only effective way to design, produce, analyse and optimise new and existing industrial thermal processes and also laser-based processes is to develop a quantitative knowledge and understanding of the dependence between temperature and time, which allow the desired forming of properties of the final products. The purpose of this paper was the performance of thermo-derivative analysis using the UMSA platform of aluminium alloy cooled at chosen rate, for obtaining characteristics used later for laser treatment and its influence on the microstructure and properties of the surface layer of heat-treated Al–Si–Cu cast aluminium alloys, using the high-power diode laser. The performed laser treatment involves remelting and feeding of ceramic powder into the aluminium surface. The carried out investigations allow to conclude that as a result of alloying of the heat-treated cast aluminium alloys with oxide ceramic powder, a surface layer was obtained with higher hardness compared to non-laser-treated material. The surface layer can be enriched with the powder particle, and in some cases a high-quality top layer is possible to obtain. Also a microstructure refinement of the surface layer was achieved due to the high laser power use and consequently high cooling rate during the crystallisation process. Concerning original practical implications of this work, there was important to investigate the appliance possibility of thermal analysis for further surface treatment for enhancement of the aluminium surface properties, especially the wear resistance and hardness. The scientific reason was also to describe microstructure changes and processes occurred in the laser remelted surface aluminium layer after laser treatment.

**Keywords** Manufacturing and processing · Surface treatment · Thermo-derivative analysis · Aluminium alloys · UMSA

## Introduction

Aluminium alloys are especially preferred in designs thanks to their good mechanical properties and possibility to make very complicated castings with high service properties. A new approach on enhancing the existing properties can be the appliance of thermo-derivative methods for further surface treatment. Nowadays aluminium alloys play an increasingly role in the world constructional material production, because of the availability and properties which are possible to obtain. Mechanical properties of the Al–Si alloys are dependent on the size, shape and distribution of the Si eutectic present in the microstructure. Improvement of the mechanical properties of these alloys is realised by general modification. Change of the fibrous Si morphology makes it possible to achieve better mechanical properties of the Al–Si alloys [1, 2].

A newly developed investigation technology is the application of derivative thermo-analysis using the

✉ Krzysztof Labisz
krzysztof.labisz@polsl.pl

[1] Faculty of Transport, Silesian University of Technology, Krasinskiego 8, 40-019 Katowice, Poland

[2] Division of Materials Processing Technology, Management and Computer Techniques in Materials Science, Institute of Engineering Materials and Biomaterials, Silesian University of Technology, Konarskiego Str 18A, 44-100 Gliwice, Poland

[3] Paint and Plastics Department, Institute for Engineering of Polymer Materials and Dyes, Chorzowska Str 50A, 44-100 Gliwice, Poland

Universal Metallurgical Simulator and Analysator. The UMSA device used for investigations is designed to overcome the existing problem of laboratory and industrial equipment on the present market. This platform combines computer controlled melting and heat treatment devices with a quench equipment, as well as the device for thermal analysis and testing equipment for in situ investigations of test sample crystallization characteristics [4–6].

This method can deliver important insight into the alloy thermal processes, which could be helpful determining the usability of the alloys for further treatment, for example surface treatment using laser. One of the modern methods for surface layer engineering is currently laser surface treatment. In this method, to the matrix there are introduced small amount of alloying additions into the surface layer in form of ceramic particle powders with different properties changing the surface layer application possibilities. The laser treatment as a part of the new generation techniques applied in metal surface technology is discussed in this paper. One of the intrinsic/distinctive high-power diode laser (HPDL) properties is the rectangular beam shape, which can be profitably used in welding of large polymer parts. Polymer welding with a single moving HPDL beam was one of the earliest applications. Welding operations can be performed simultaneously when a single scanable beam is replaced by several larger rectangular beams. HPDL is the most productive artificial light sources which a significant part of the electrical energy is converted to heat in the diode laser.

In real conditions, the crystallization of the Al alloys shows departures of the crystallization process resulting from the Al–Si equilibrium diagram, which is a binary system with an eutectic and limited solubility of the components in a solid state. The reason of this difference is the considerably higher alloy crystallization rate, compared to this occurred in equilibrium conditions, but also the change in the initial alloy microstructure in the liquid state, caused by impurities, or specially added modifiers for the reason of microstructure modification and morphology changes of the ($\alpha$Al + $\beta$Si) eutectic or shifting of the characteristic equilibrium diagram temperature points, because of the pressure increase during the alloy crystallisation process. In this area, also the HPDL laser treatment with ceramic particle feeding is of big importance for changing the microstructure of aluminium [7–14]. The field of use of such HPDL-treated surface is repair of working elements produced from aluminium, where enhanced hardness and wear resistance is of great importance, for example valve seats or motor housing and pulley system parts.

Exact knowledge of the impact of the cooling rate applied for die castings on the microstructure and phase transition temperature during non-equilibrium crystallization allows optimal control of the production process. The separation of the derivative curve definitions to basic functions allows accurate calculation of latent crystallization heat of various phases crystallising during solidification. Assuming that the latent crystallization heat is proportional to the share of the various phases in the alloy, the thermo-derivative analysis also allows the calculation of the amount of crystallised phases. Calculation of the above-mentioned properties is based on the characteristic points determined in a derivative curve. These points are usually reflecting the thermal effects occurring in the melt during crystallization and are dependent on the alloy composition, cooling rate, heat generation rate and crystallization temperature of the molten metal, and so the parameters affecting the final microstructure of the resulting alloy. These parameters characterise also the crystallization kinetics of the alloys.

The general equation, describing (Table 1) the crystallisation function as a derivative of the crystallisation, is given as (1) [3, 4]:

$$\frac{\mathrm{d}T}{\mathrm{d}t} = \frac{A}{m \times c_\mathrm{p}} \times \alpha(t) \times (T - T_0) + \frac{K_\mathrm{K}}{m \times c_\mathrm{p}} \times \left( m\frac{\mathrm{d}z}{\mathrm{d}t} + z\frac{\mathrm{d}m}{\mathrm{d}t} \right) \quad (1)$$

The basic laser treatment parameters are the practical aim of this work, as well as improvement of hardness. Special attention was payed to studying of the surface layer morphology of the investigated material especially the surface layer microstructure [15–30] if the used ceramic particle powder was properly introduced into the matrix, how the phases were changed in terms of distribution and size as well as if a zone-like structure was obtained after appliance of the laser surface treatment.

## Experimental

The material used for investigation was the $AlSi_7Cu$ and $AlSi_9Cu_4$ aluminium alloys. The chemical compositions of the investigated aluminium alloys are presented in Table 2, as obtained by the manufacturer. For feeding of both of the material types, the zirconium oxide $ZrO_2$ and titanium

**Table 1** Description of the equation factors

| Symbol | Descriptions |
|---|---|
| $c_\mathrm{p}$ | Heat capacity |
| $m$ | Mass of the crystallised metal |
| $T$ | Temperature at time d$t$ |
| $T_\mathrm{O}$ | Environment temperature |
| $A$ | Sampler surface |
| $K_\mathrm{K}$ | Crystallisation constant |
| $z$ | Nucleus number |

**Table 2** Chemical composition of the investigated aluminium alloys

| Elements | Chemical composition | |
|---|---|---|
| Alloys | $AlSi_7Cu$ | $AlSi_9Cu_4$ |
| Si | 7.17 | 7.45 |
| Fe | 0.14 | 0.17 |
| Cu | 0.99 | 3.60 |
| Mn | 0.11 | 0.25 |
| Mg | 0.27 | 0.28 |
| Zn | 0.05 | 0.06 |
| Ti | 0.08 | 0.13 |
| Al | Balance | Balance |

Chemical composition of the investigated alloys, in mass %

carbide TiC mixed powders were used in a ration 50–50% by a fluidisation feeder mounted on the lasers head.

The heat treatment for both alloys was carried out in the electric resistance furnace U117, with a heating rate of 80 °C $s^{-1}$ for the ageing process and 300 °C $s^{-1}$ for the solution heat treatment process with two holds at 300 and 450 °C performed for 15 min. Parameters of the solution heat treatment process and ageing process are presented in Table 3.

Thermo-analysis of the investigated alloy was carried out using UMSA device. The heating and cooling system, with experimental conditions, is presented in Fig. 1. The samples were cooled using compressed gas supplied through the nozzles present in the heating inductor. The gas flowing rate for sample cooling was regulated and controlled using a rotameter. The compressed gas flow rate was regulated for achieving the cooling rate of 0.1 °C $s^{-1}$ for furnace cooled sample.

For measurement, K-type (chromo–alumel) thermocouples were used. Tests were performed several times for each cooling rate for statistical estimation of the investigation results.

High-power diode laser HPDL Rofin DL 020 was used for remelting. The used laser is a device with high power, used in materials science, including for welding. The laser equipment contained: rotary table which moving in the XY plane, the nozzle of the powder feeder for the enrichment

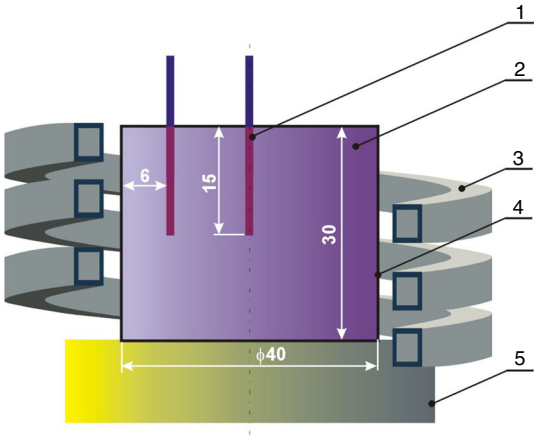


**Fig. 1** UMSA device location scheme of the heating and cooling system, as well as size of the samples for thermo-analysis: (*1*) thermocouple, (*2*) heating inductor—cooling nozzles, (*3*) steel foil, (*4*) sample, (*5*) sampler isolation

or welding, shielding gas nozzle, laser head, power system, cooling system and the computer system controlling the operation and location of the laser. The powder feed rate was chosen as 1 g $min^{-1}$ and the laser scan rate 0.5 m $min^{-1}$. Working parameters of the HPDL Rofin DL 020 are shown in Table 4.

For determining the influence of cooling rate on the further surface layer properties, the following investigations were carried out:

- Thermo-derivative analysis using the UMSA thermo simulator (Fig. 1).
- The micrographs of the microstructure investigation were performed using the light microscope Leica MEF4A supplied by Zeiss in a magnification range of 50–500 times. The micrographs of the microstructures were made by means of the KS 300 program using the digital camera equipped with a special image software. Also the intern image calculation software was used for calculation of the phases present in the microstructure.
- The obtained results from the microstructure investigation were performed on the scanning electron microscope ZEISS Supra 35 with a magnification up to 2500 times, as well as on a transmission electron

**Table 3** Heat treatment parameters

| Ageing process | | Solution heat treatment | |
|---|---|---|---|
| Temperature | 175 °C for 12 h | Temperature | 505 °C for 10 h |
| Heating rate | 80 °C $s^{-1}$ | Heating rate | 300 °C $s^{-1}$ |
| Isothermal holds | 450 °C by 15 min | Isothermal holds | 450 °C by 15 min |
| Isothermal holds | 300 °C by 15 min | Isothermal holds | 300 °C by 15 min |
| Cooling medium | Air | Cooling medium | Water |

Heat treatment parameters used for the investigated $AlSi_9Cu_4$ and $AlSi_7Cu$ alloys

**Table 4** HPDL laser working parameters

| Parameter | Value |
|---|---|
| Laser wavelength/nm | 940 ± 5 |
| Peak power/W | 100 + 2300 |
| Focus length of the laser beam/mm | 82/32 |
| Power density range of the laser beam in the focus plane/kW $(cm^2)^{-1}$ | 0.8/36.5 |
| Dimensions of the laser beam focus/mm | 1.8 × 6.8/1.8 × 3.8 |
| Laser scan rate/m $min^{-1}$ | 2 |
| Powder feed rate/g $min^{-1}$ | 5 |

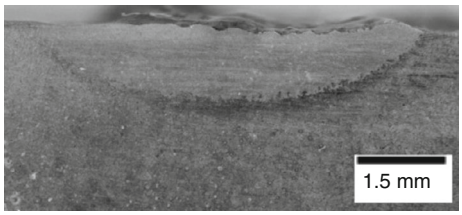


**Fig. 2** Cross section of the investigated $AlSi_9Cu_4$ surface layer after laser treatment $ZrO_2$ + TiC, laser power 1.5 kW

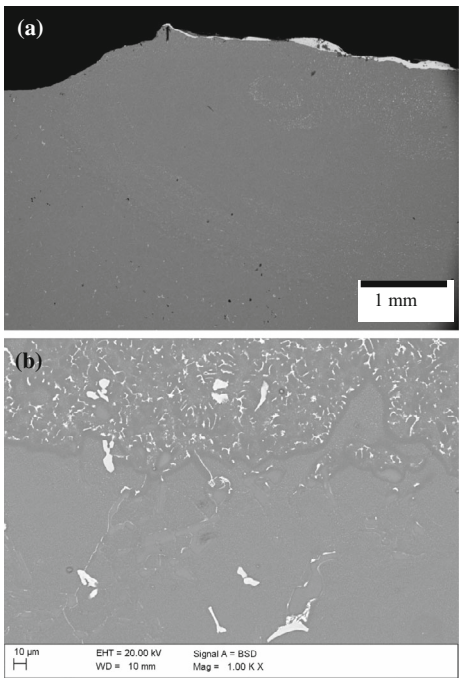


**Fig. 3** Microstructure of the investigated $AlSi_7Cu$ alloy, $ZrO_2$ + TiC, 1.5 kW (**a**), transition zone between the heat influence zone and the substrate material (**b**)

microscope with the high-angle annular dark-field (HAADF) mode. For microstructure evaluation, the back-scattered electrons (BSE) as well as the secondary

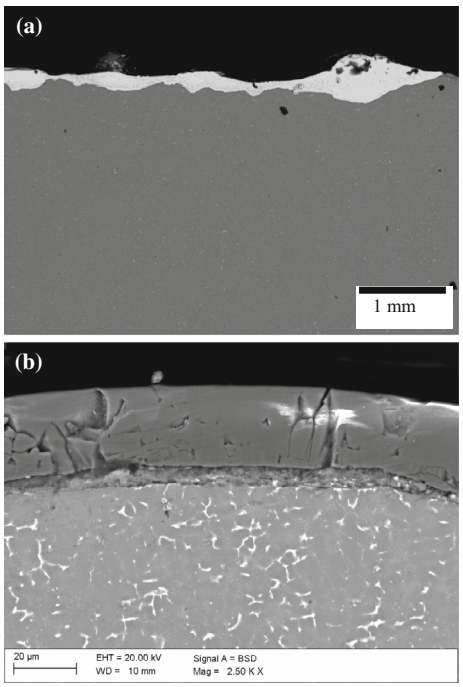


**Fig. 4** Microstructure of the investigated $AlSi_9Cu_4$ alloy, $ZrO_2$ + TiC, 1.5 kW (**a**), transition zone between the remelting zone and heat influence zone (**b**)

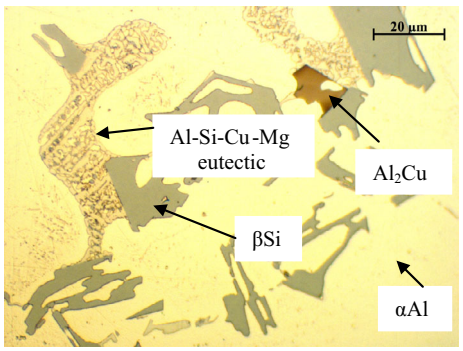


**Fig. 5** Microstructure of the $AlSi_9Cu_4$, as-cast state, cooled sample with 0.1 °C $s^{-1}$

electron (SE) detection method was used, with the accelerating voltage of 20 kV.

- The hardness was measured with Rockwell hardness tester with a load chosen for the HRF scale, with a load of 600 N, predestined for light alloy hardness testing.

## Results and discussion

The obtained results from the microstructure investigation performed on scanning electron microscope ZEISS Supra 35 with a magnification up to 500 times reveal the cross-sectional

structure (Fig. 2) of the surface layer, revealing the remelting zone (RZ) as well as the presence of the used $ZrO_2$ powder in form of a film (Figs. 3, 4)—discontinuous for the $AlSi_7Cu$ alloy. In case of this powder, the particles are sintered building a layer on the top of the laser-treated aluminium surface and are not emerged in the matrix. For microstructure evaluation, the back-scattered electrons (BSE) detection method was used, with the accelerating voltage of 20 kV.

The morphology of the resulting quasi-composite layer tends to be not homogeny and entered the correct dispersion of particles throughout the depth of penetration with the exception of a very thin layer of diffusion saturation; therefore, it is very important to know which structural features and microstructure elements can be present in different thermal conditions.

The occurred discontinuity of the layer can be seen as a product of the heat transfer process and may be neutralised by properly adjusted powder quality and powder feed rate. It is also possible on the basis of these cross-sectional micrographs to evaluate the thickness of the surface layer

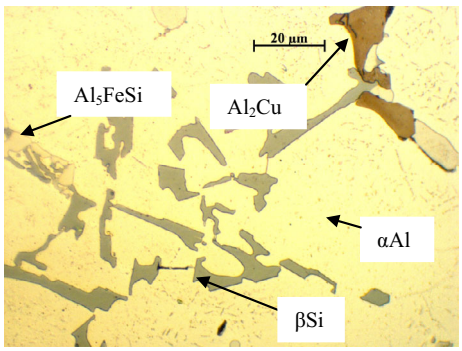


**Fig. 6** Microstructure of the $AlSi_7Cu$, as-cast state, cooled sample with 0.1 °C $s^{-1}$

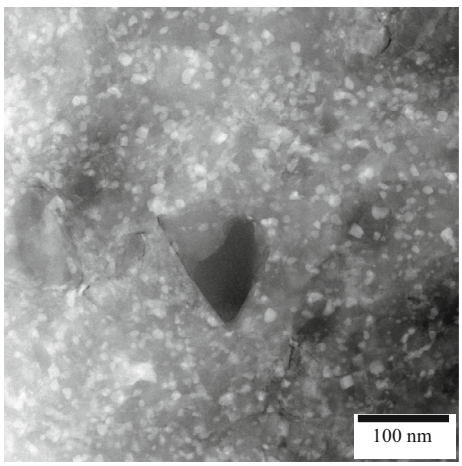


**Fig. 7** Microstructure of the investigated Al alloy, revealing the $Mg_2Si$ phase, HAADF-TEM

depth, which is ca. 0.7 µm (Fig. 9) in case of the $AlSi_9Cu_4$ alloy. For the $AlSi_7Cu$ alloy, the obtained microstructure investigation results allow to confirm only a minor amount of the $ZrO_2$ powder on the surface of the treated alloy. It was also found that the examined layers consist of three

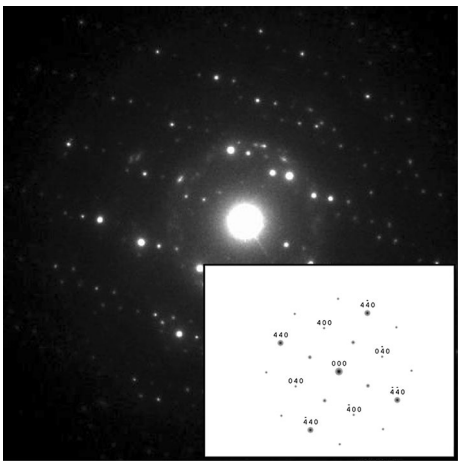

**Fig. 8** Electron diffraction pattern forms the phase in Fig. 7, with solution for the $Mg_2Si$ phase, [001] zone axis, TEM

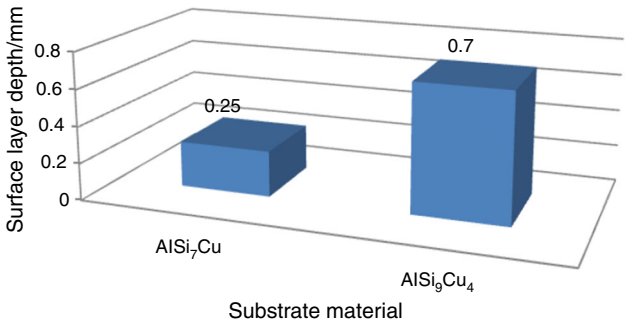


**Fig. 9** Surface layer depth measurement results of the alloyed cast aluminium alloys with $ZrO_2$/TiC ceramic powder

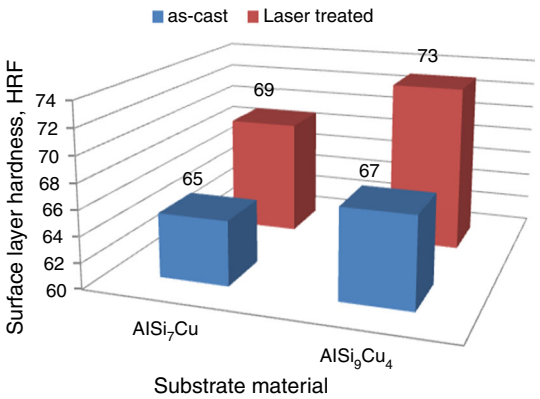


**Fig. 10** Surface layer hardness measurement results of the alloyed cast aluminium alloys with $ZrO_2$/TiC ceramic powder

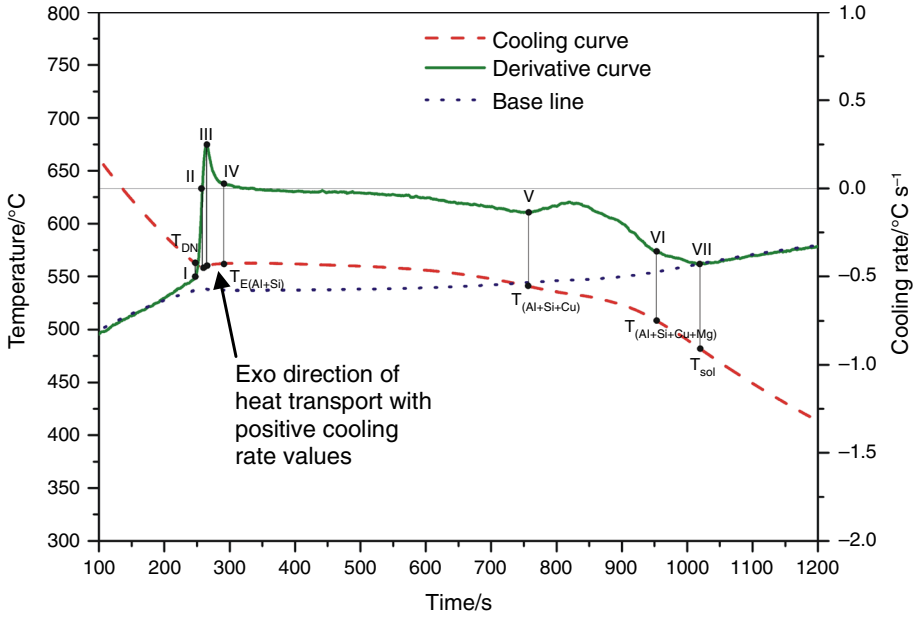


**Fig. 11** Thermo-derivative analysis of the $AlSi_7Cu$ alloy

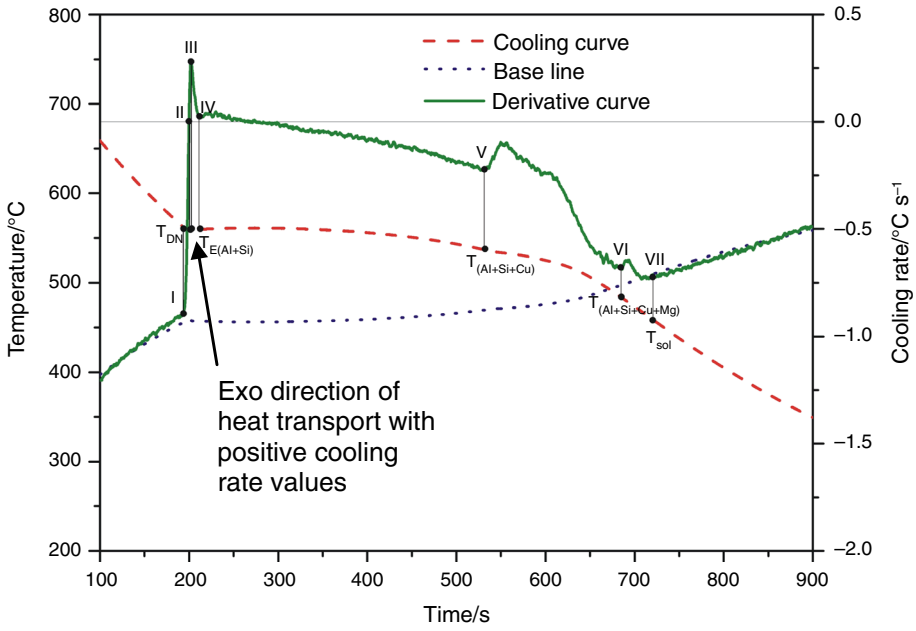


**Fig. 12** Thermo-derivative analysis of the $AlSi_9Cu_4$ alloy

subzones—the remelted zone, the heat influence zone and the substrate material. Further investigations will be needed to reveal the morphology and nature of these zones, occurring after alloying with different process parameters and different ceramic powders.

It is known that the coarseness of the as-cast microstructure (Figs. 5, 6) clearly affects the solution treatment time needed to dissolve particles and obtain a homogenous distribution of alloying elements in the matrix. A short solution treatment time of 10 min is enough to achieve a high and homogenous copper concentration for a material with a fine microstructure.

There is also a different phase composition in the thermally treated alloys; in case of the as-cast $AlSi_7Cu$ alloy, there are common $Al_5FeSi$ and $Al_2Cu$ phases present, whereas in the $AlSi_9Cu_4$ alloy occurs also in a higher amount of the AlSiCuMg multiphase eutectic, consisting of the $Al_2Cu$ and $Al_5FeSi$ phases, as well as of a magnesium and silicon-containing phase $Mg_2Si$ (Figs. 7 and 8).

The uneven areas and hollows in the surface layer of the Al–Si-Cu alloys with laser-alloyed zirconium oxide particles are produced as a result of intensive heating of the surface. Depending on the type of substrate, laser power, feed rate and the powder applied, the surface on which high

**Table 5** Description of the characteristic points on the cooling curve from Figs. 9 and 10

| Point on the graph | Description |
|---|---|
| I | $T_{DN}$ nucleation temperature |
| II | $T$ temperature of the beginning of the crystal growth (α phase dendrites) |
| III | Dendrites (α phase) growth temperature |
| IV | Temperature of α phase dendrite growth and (αAl + βSi) precipitation growth |
| V | Nucleation temperature of the (Al–Si–Cu) eutectics |
| VI | Nucleation temperature of the (Al–Si–Cu–Mg) multiphase eutectic |
| VII | $T_{Sol}$ temperature of the crystallization end |

gradient of surface tension is produced is unevenly heated, which has a direct influence on the formation of the melted material in the remelting lake.

Some of the alloy and ceramic parts embedded in the remelting zone are evaporated under high temperature occurring during laser treatment; therefore, the characteristic hollows appear on the remelting surface. It was also found that, disregarding the ceramic powder used, in the laser bundle power range from 1.2 to 2.0 kW the porosity of the obtained composite layers increases, in comparison with that of the raw cast surfaces of aluminium alloys.

The silicon particles, present as coarse, acicular needles under normal cooling conditions, act as crack initiators but enhance the hardness. A higher influence on the hardness increase can be observed based on the comparison between as-cast and HPDL-treated samples, where for the laser-treated sample the hardness increase an even more clear, equal 73 HRF for the $AlSi_9Cu_4$ alloy, influenced also by higher grain refinement (Fig. 10).

There is obviously a clear relationship between the laser power applied and the achieved quality of the laser-treated surface, and the particular investigation concerning laser power influence were carried out in former works [3, 4]. It was found that the optimal laser power is ca. 1.5 kW.

Higher addition of silicon and copper in alloy caused change in the derivative curve (Figs. 11, 12). Higher amount of silicon and copper affects the position of the characteristic points of the beginning and end of solidification of the eutectic phases. Figure 11 shows an example of the cooling curves and derivative curves of the $AlSi_7Cu$ alloys. In this case, there is no evidence of occurring of any other phases than commonly known, whereas for the $AlSi_9Cu_4$ alloy there is a clear area in the curve marked with points VI (nucleation temperature of the (Al–Si–Cu–Mg) multiphase eutectic) (Table 5) where the multiphase eutectic occurs. Change of the derivative curve effects also the area under the curve and the ratio of the various phases and eutectic according to the chemical composition and cooling rate. For example, for the $AlSi_9Cu_4$ alloy the occurrence of the Al–Si–Cu–Mg eutectic was confirmed, as well as the amount of the Si phase was measured as 8.43% compared to 5.64% for the $AlSi_7Cu$ alloy.

Very important issue is also the crystallisation end temperature for the investigated alloys. This $T_{Sol}$ temperature is ca 465 °C for the $AlSi_7Cu$ alloy and ca 455 °C for the $AlSi_9Cu_4$ alloy. The maximal heating temperature is much more higher than the $T_L$ (liquidus) temperature for both types of the investigated alloys because of the necessity to have information about the solidification process and phase transformations occurred on the beginning of the alloy solidification—ca. 650 °C for the beginning of the crystal growth (α phase dendrites). Such high temperature was also chosen, because of the following laser treatment, where the metal surface if entire remelted, and some crystallization process could have placed in higher temperature, compared to the classical phase transformation diagram.

On the basis of these data, an undercooling for this alloy can be stated, where the alloy solidifies in lower temperature, than given in the equilibrium diagram. Such undercooling occurs also after the laser alloying of the surface layer, where the temperature reaches even 3000 °C. So a higher amount of alloying additives can lead to a presence of the phase composition of the alloy and a higher possibility for heat transfer, by this way alloys with higher alloying element content, and also impurities are more likely to be used for laser surface treatment.

## Conclusions

Control of the hypo-eutectic alloy microstructures is imperative in the design of both superior hardness tribological properties at the bore surface and for exceptional mechanical strength. However, the solidification kinetics and the sequence of the phase transformations in relation to the as-cast and heat-treated microstructure needs still to be further understood, quantified and implemented for further improvement of the casting technology and cast component service characteristics. The performed investigations of the microstructure evaluation of the Al–Si–Cu alloys, carried out using light and scanning electron microscope, allow to confirm the zone-like nature of the surface layer obtained using HPDL laser for alloying of the $AlSi_7Cu$ as well as the $AlSi_9Cu_4$ cast aluminium alloys. There were revealed also a zone-like nature on the top of the substrate material, like: the remelting zone and the heat influence zone.

The investigated hypo-eutectic Al–Si alloys are near eutectic Al–Si alloys with the addition of copper and small addition of iron and magnesium, reveal the occurrence of formation of aluminium reach (α-Al) dendrites followed by development of three phases which are of importance for achieving the required properties after properly performed heat treatment, these are: the Si phase, the $Al_2Cu$ phase as well as the $Al_5FeSi$ phase. However, the additional alloying elements Fe, Mg, Cu lead to more complex solidification reaction, partially unidentified.

Crystallization of the investigated Al–Si alloy starts with the crystallization of α-Al, followed by αAl + βSi eutectic; silicomanganese FeSiMn phase. There are some indices, mainly on the thermal analysis curve, that some less often occurred phases are present in this alloy for example the $Mg_2Si$ phase, which was confirmed using the electron diffraction method on the transmission electron microscope.

Cooling rate has an important influence on the hardness, which has a value of 73 HRF for the samples cooled with 0.1 °C $s^{-1}$.

Particularly, it was found that:

1. The optimal laser power is in the range of <1.0–2.0> kW.
2. The $ZrO_2$\TiC powder particles do not feed into the aluminium alloy matrix during laser alloying, instead there is formed a sintered $ZrO_2$ layer onto the investigated aluminium cast alloy, the presence of the titanium carbide phase could not be detected in the microstructure or using EDS analysis. It is probably evaporated during the laser feeding process.
3. The $AlSi_9Cu_4$ alloy has a more homogeny surface layer depth after alloying compared to the $AlSi_7Cu$ aluminium alloy.

The laser power determination leads to the conclusion, that the optimal power range is ca. 1.5 kW, a lower value of ca 1.0 kW does not lead to achievement of an completely homogeny remelting tray on the sample surface, whereas a to high power of 2.0 kW makes an uneven, bumpy or hilly shape of the remelted area.

**Acknowledgements** This publication was financed by the Ministry of Science and Higher Education of Poland as the statutory Financial Grant of the Faculty of Mechanical Engineering SUT. This research was also partially financed partially within the framework of the Scientific Research Project No. 2011/01/B/ST8/06663 headed by Dr. KL.



## References

1. Dobrzański LA, Krupiński M, Labisz K, Krupińska B, Grajcar A. Phases and structure characteristics of the near eutectic Al–Si–Cu alloy using derivative thermo analysis. Mater Sci Forum. 2010;638–642:475–80.
2. Yang LJ. The effect of casting temperature on the properties of squeeze cast aluminium and zinc alloys. J Mater Process Technol. 2003;140:391–6.
3. Krupinski M, Krupinska B, Rdzawski Z, Labisz K, Tanski T. Additives and thermal treatment influence on microstructure of nonferrous alloys. J Therm Anal Calorim. 2015;120:1573–83.
4. Krupinski M, Krupinska B, Labisz K, Rdzawski Z, Tanski T. Effect of chemical composition modification on structure and properties of the cast Zn–Al–Cu alloys. Proc IME J Mater Des Appl. 2016;230:805–12.
5. Tański T, Dobrzański LA, Cizek L. Influence of heat treatment on structure and properties of the cast magnesium alloys. Adv Mater Res. 2007;15–17:491–6.
6. Konieczny J, Dobrzański LA, Labisz K, Duszczyk J. The influence of cast method and anodizing parameters on structure and layer thickness of aluminum alloys. J Mater Process Technol. 2004;157–158:718–23.
7. Choudhury P, Das S. Effect of microstructure on the corrosion behaviour of a zinc–aluminium alloy. J Mater Sci. 2005;40:805–7.
8. Alcock CB, Itkin VP. The Al–Sr (aluminum–strontium) system. Bull Alloy Phase Diagr. 1989;10(6):624–30.
9. Mazhar AA, Salih SA, Gad-Allah AG, Tammam RH. Corrosion inhibition of Zn–Al–Cu alloy by 2-aminothiazole. JMEPEG. 2008;17:260–70.
10. Yang LJ. The effect of solidification time in squeeze casting of aluminium and zinc alloys. J Mater Process Technol. 2007;192–193:114–20.
11. Kang N, Na HS, Kim SJ, Yun C, Kang CY. Alloy design of Zn–Al–Cu solder for ultra-high temperatures. J Alloy Compd. 2009;467:246–50.
12. Balout B, Masounave J, Songmene V. Modeling of eutectic macro segregation in centrifugal casting of thin walled ZA8 zinc alloy. J Mater Process Technol. 2009;209:5955–63.
13. Chen TJ, Hao Y, Sun J, Li YD. Effects of Mg and RE additions on the semi-solid microstructure of a zinc alloy ZA27. Sci Technol Adv Mater. 2003;4:495–502.
14. Labisz K. Microstructure and mechanical properties of high power diode laser (HPDL) treated cast aluminium alloys. Materialwissenschaft und Werkstofftechnik. 2014;45:314–24.
15. Tański T. Determining of laser surface treatment parameters used for light metal alloying with ceramic powders. Materialwissenschaft und Werkstofftechnik. 2014;45:333–43.
16. Dobrzański LA, Labisz K, Piec M, Lelątko J, Klimpel A. Structure and properties of the $_{32}CrMoV_{12\text{-}28}$ steel alloyed with WC powder using HPDL laser. Mater Sci Forum. 2006;530–531:334–9.
17. Piec M, Dobrzański LA, Labisz K, Jonda E, Klimpel A. Laser alloying with WC ceramic powder in hot work tool steel using a high power diode laser (HPDL). Adv Mater Res. 2007;15–17:193–8.
18. Dae-Hwan K, Seong-Hyeon H, Byoung-Kee K. Fabrication of ultrafine TaC powders by mechano-chemical process. Mater Lett. 2004;58:87–92.
19. Tański T, Labisz K. Structure and properties of diamond-like carbon coatings deposited on non-ferrous alloys. Solid State Phenom. 2013;199:170–5.
20. Tański T, Dobrzański LA, Cizek L. Influence of heat treatment on structure and properties of the cast magnesium alloys. Adv Mater Res. 2007;15–17:491–6.

21. Lisiecki A, Klimpel A. Diode laser gas nitriding of $Ti_6Al_4V$ alloy. Arch Mater Sci Eng. 2008;31:53–6.
22. Gwoździk M, Nitkiewicz Z. Analysis of crystallite size and lattice deformations changes in an oxide layer on P91 steel. Arch Metall Mater. 2013;58:31–4.
23. Gwoździk M, Nitkiewicz Z. Studies on the adhesion of oxide layer formed on $X_{10}CrMoVNb_{9\text{-}1}$ steel. Arch Civ Mech Eng. 2014;14:335–41.
24. Dobrzański LA, Borek W. Thermo-mechanical treatment of Fe–Mn–(Al, Si) TRIP/TWIP steels. Arch Civ Mech Eng. 2012;12:299–304.
25. Rusz S, Dutkiewicz J, Faryna M, Maziarz W, Rogal L, Bogucka J, Malanik K, Kedroň J, Tylšar S. SEM EBSD and TEM structure studies of α-brass after severe plastic deformation using equal channel rolling followed by groove pressing. Solid State Phenom. 2012;186:94–7.
26. Grabowska B, Malinowski P, Szucki M, et al. J Therm Anal Calorim. 2016;126:245. doi:10.1007/s10973-016-5435-5.
27. Farahany S, Idris MH, Ourdjini A, Faris F, Ghandvar H. Evaluation of the effect of grain refiners on the solidification characteristics of an Sr-modified ADC12 die-casting alloy by cooling curve thermal analysis. J Therm Anal Calorim. 2015;119:1593–601.
28. de Oro Calderon R, Gierl-Mayer C, Danninger H. Application of thermal analysis techniques to study the oxidation/reduction phenomena during sintering of steels containing oxygen-sensitive alloying elements. J Therm Anal Calorim. 2016. doi:10.1007/s10973-016-5508-5.
29. Pędrak P, Drajewicz M, Dychtoń K, et al. Microstructure and thermal characteristics of $SiC–Al_2O_3$–Ni composite for high-temperature application. J Therm Anal Calorim. 2016;125:1353. doi:10.1007/s10973-016-5608-2.
30. Wrobel G, Szymiczek M, Wierzbicki L. Swagelining as a method of pipelines rehabilitation. J Mater Process Technol. 2005;157:637–42.